ACS APPLIED MATERIALS & INTERFACES

Research Article

www.acsami.org

Plasmon-Induced Efficiency Enhancement on Dye-Sensitized Solar Cell by a 3D TNW-AuNP Layer

Yin-Cheng Yen, Po-Hung Chen, Jing-Zhi Chen, Jau-An Chen, and Kuan-Jiuh Lin*

Department of Chemistry, National Chung Hsing University, Taichung 40227, Taiwan, Republic of China

Supporting Information

ABSTRACT: A new 3D TNW-AuNP plasmonic electrode consists of antireflective (AR) TiO_2 nanowires (TNWs) (~600 nm thickness) serving as light-harvesting antennae coupling with Au nanoparticles (NPs). A huge red-shift of 55 nm is observed in surface plasmon spectra for the Au (11 nm) plasmonic electrode that has 11 nm size Au NPs, whereby (111) lattice planes have a specific bonding with the TiO_2 (101) planes. Remarkable red-shift is mainly attributed to the localized electric field improvement resulting from the plasmonic coupling effect between the Au NPs and the Au−TiO_2 hybrids. After $TiCl_4$ treatment, this favorable Au (11 nm) nanostructure takes advantage of harvesting photons to increase the conversion efficiency of dye-sensitized solar cells (DSSCs) from 6.25% to 9.73%.

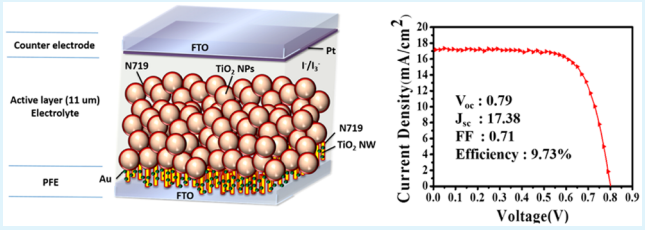

KEYWORDS: *gold, TiO_2 nanowire, dye-sensitized solar cell, LSPR, antireflection, light-harvesting*

AR films with light trapping characteristics played a pivotal role in enhancing the efficiency of photovoltaic devices.[1] For Si photovoltaic devices, surface textured AR coatings with porosity and roughness could take advantage of light trapping to increase the absorbance.[2−4] For thin-film devices, AR films generally consist of more dielectric layers to improve light trapping performance, giving a more broadband response in reflection.[5,6] In the ongoing single-layer AR coating revolution, we previously successfully utilized a low-temperature (80 °C) method on the growth of a single layer (~600 nm) of TNWs onto fluorine tin oxide (FTO) substrates.[7] Ascribing to the characteristically random standing and highly porous structure of the TNWs, the refractive index (RI) of TiO_2 film can be effectively reduced to approximately 1.22−1.51 as compared to 2.5 in TiO_2 bulk material. Thus, a splendid antireflection property on glass substrates is performed, and large transmittance enhancement (6−8%) can be observed. From an antenna perspective, these AR TiO_2 nanowired FTO-electrodes can be used to exploit the benefits of light by decorating plasmonic metal nanostructures for creating new types of clean solar-energy harvesting devices.

To make more attractive potential features of dye-sensitized solar cells (DSSCs), plasmonic functionalized electrodes (PFEs), engineering of noble metallic NPs modified TiO_2-electrodes has been extensively researched for light-harvesting systems because of plasmon coupling effects: excitation of the conduction electrons at the interface between a metal and a dielectric.[8−12] However, these reports mainly discuss the effects on the amount, size, and shape of metallic NPs in the thick TiO_2 films (4−12 um). Recently, one novel example of plasmonic coupling by TiO_2-induced electric field was proposed by Wang et al. An Au/TiO_2/Au nanostructure with a 5 nm thick TiO_2 middle layer was synthesized, which satisfies the requirement of the distance for generating the coupling effect between the opposite and nearly touching Au NPs on Ti foils.[13] According to this report, the finite-difference time domain (FDTD) result shows that the Au/TiO_2/Au nanosheet configuration has a maximum 38-fold enhancement on electric field density arising from the polarization-dependent coupling effect between Au NPs. However, this type of electrode was limited in photovoltaic devices due to its poor degree of light absorption in the active layer. Therefore, how to design, fabricate, and tailor the optical properties of new typed PFE is indispensable in utilizing a large fraction of the solar spectrum and then enhancing the conversion efficiency. To improve photovoltaic performance, herein we carry out the growth of Au (111) NPs in the TiO_2 nanowired FTO, a new configuration of 3D TNW-AuNP plasmonic electrodes (Figure 1) that possess a dual nature of AR characteristic and plasmon coupling effect leading to remarkably enhanced light-harvesting efficiency.

The cross-sectional and surface field-emission scanning electron microscope (FESEM) images of TNW were, respectively, shown in Figure 2a and b, which shows a film length of 600 nm and a highly porous phenomenon indicative of typical AR characteristics (see Supporting Information Figure S1).[7] Afterward, PFEs made of hybrid TNW-AuNP were carried out using a simple Au-film calcination approach. Briefly, after calcinating at 500 °C for 30 min, the as-prepared 2.5, 5, and 10 nm-thick Au films were converted into plasmonic

Received: November 3, 2014
Accepted: December 30, 2014
Published: December 30, 2014

DOI: 10.1021/am507668j
ACS Appl. Mater. Interfaces 2015, 7, 1892−1898

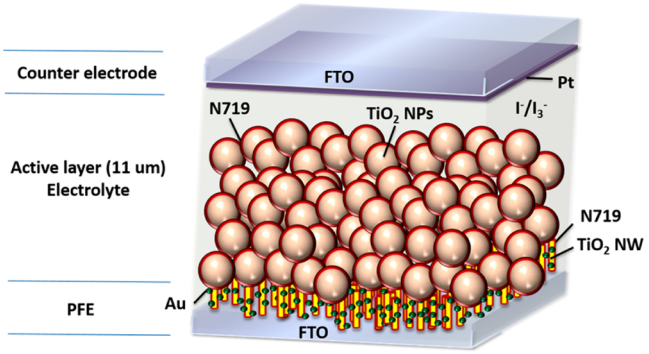

Figure 1. Schematic of the PFE in DSSC devices. PFE consisted of AR TNW (less than 600 nm) and Au NPs onto FTO substrate.

NPs with size of 11, 19, and 37 nm, respectively. Their corresponding FESEM images for TNW-AuNP PFEs, denoted as Au (11 nm), Au (19 nm), and Au (37 nm), were, respectively, shown in Figure 2c–e. Moreover, their NP size distributions are shown in Figure 2f. It is clearly observed that the thickness of as-prepared Au films played an important role in the size control of Au NP formation on TNWs. The average Au NPs size was increased from 11 to 37 nm along with the as-prepared Au film thickness from 2.5 to 10 nm. Here, we proposed the formation mechanism from Au film to Au NPs, shown in Figure 3a. Before calcination, we observed that the rough Au layer was deposited on the surface of TNW, Figure 3b. After calcination at 500 °C for 15 min, the Au layer melted and ruptured into many small fragments (Figure 3c) because of the small size effect of nanomaterials and the unmatched thermal expansion coefficients between the Au layer and TNWs. After calcination for 30 min, due to the surface tension effect, the Au fragments shrink into many Au NPs (Figure 2d).

The localized surface plasmon resonance (LSPR) properties of the TNW-AuNP PFEs are provided in Figure 4. As seen in Figure 4a, the LSPR peaks for Au (11 nm), Au (19 nm), and Au (37 nm) are of 575, 567, and 550 nm, respectively. It should be noted that a remarkable red-shift was observed in the LSPR of the Au (11 nm), which has the smallest size of Au NPs on TNWs. It was given that the bare Au NPs with 10 nm size on glass substrate exhibited a LSPR peak around 520 nm.[14] The plasmonic wavelength of Au (11 nm) system is obviously shifted to 575 nm, even larger than those of the other two larger Au NPs cases (Au (19 nm), 567 nm; Au (37 nm), 550 nm). A remarkable red-shift of 55 nm is obtained in the case of the Au (11 nm). This is contrary to the tendency of size effect in LSPR theory. Two factors are probably responsible for the red-shift behavior. First, a synergistic interaction between the Au NPs and the TNWs can cause a red-shift. Generally, LSPR wavelength strongly depends on the particle size and their coupling interaction with dielectric medium substrates[15−17] based on the equation, $\lambda_{sp} = 2\pi c(\varepsilon_0 m_e(\varepsilon_\infty + kn_m^2)/Ne^2)^{1/2}$, where κ is a NP geometry-dependent factor (e.g., $\kappa = 2$ for a

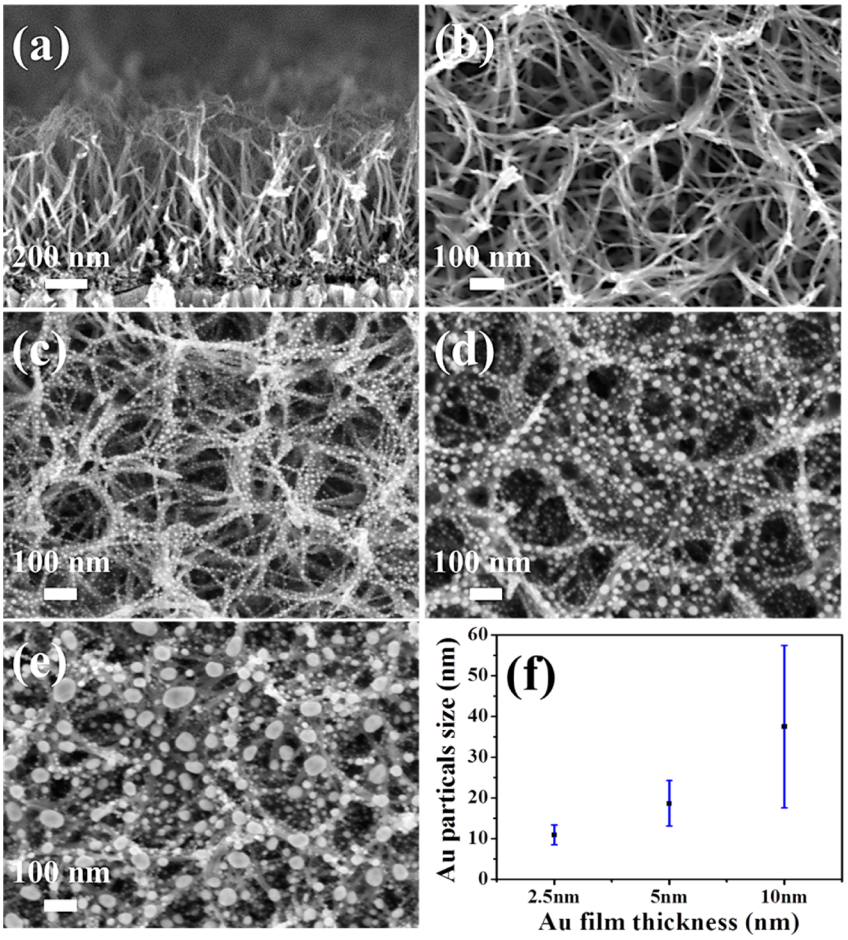

Figure 2. (a) Cross-section and (b) top-surface FESEM images of TNWs. FESEM images of TNW-AuNP PFEs: (c) Au (11 nm), (d) Au (19 nm), and (e) Au (37 nm). (f) The corresponding particle size distributions of Au (11 nm), Au (19 nm), and Au (37 nm).

DOI: 10.1021/am507668j
ACS Appl. Mater. Interfaces 2015, 7, 1892−1898

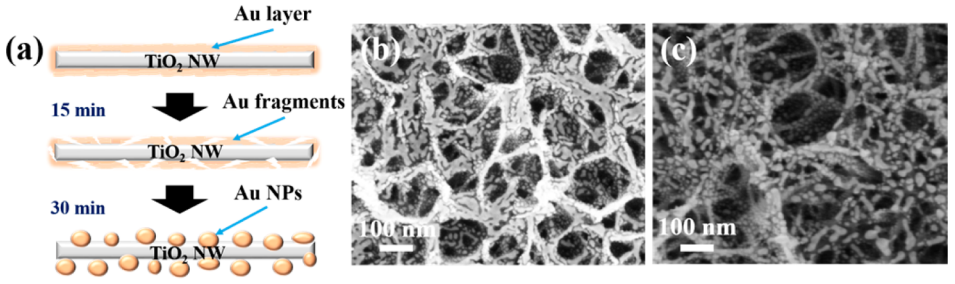

Figure 3. (a) Formation mechanism of Au NPs. Top-surface FESEM images of TNW-Au layer (with thickness of 5 nm) (b) without calcination and (c) with calcination for 15 min.

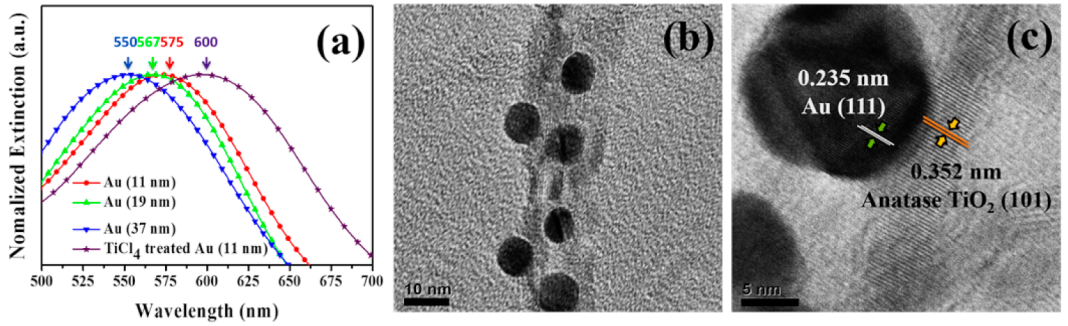

Figure 4. (a) LSPR spectra for TNW-AuNP PFEs. (b) High-resolution transmission electron microscope (HRTEM) image and (c) lattice fingers of Au (11 nm).

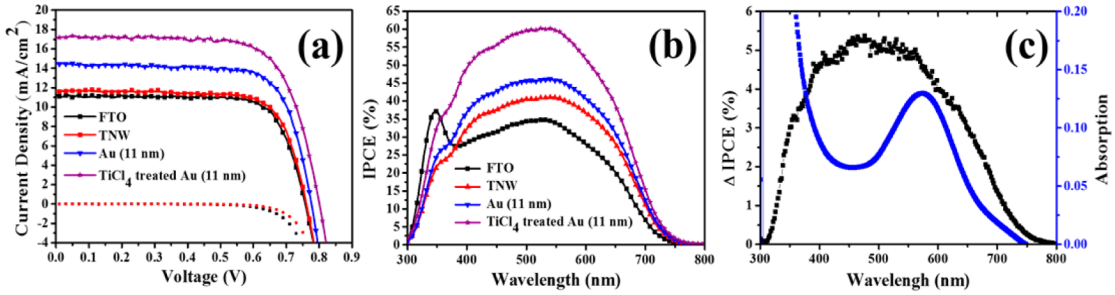

Figure 5. (a) $J-V$ cures and (b) IPCE profiles of PFE-based DSSCs. (c) Delta IPCE plots of Au (11 nm) in the incident wavelength between 300 and 800 nm. The corresponding absorption spectra of Au (11 nm) are also included for comparison.

Table 1. PV Characterizations of PFE-Based DSSCs under Simulated AM1.5 Sunlight (100 mW cm^{-2})[a]

electrodes	V_{oc} (V)	J_{sc} (mA cm^{-2})	FF	efficiency (%)
FTO	0.76 ± 0.02	10.91 ± 0.76	0.76 ± 0.02	6.25 ± 0.15
TNW	0.77 ± 0.01	11.66 ± 0.32	0.74 ± 0.01	6.62 ± 0.10
Au (11 nm)	0.78 ± 0.01	14.64 ± 0.35	0.74 ± 0.01	8.39 ± 0.31
Au (19 nm)	0.77 ± 0.00	12.69 ± 0.37	0.74 ± 0.01	7.19 ± 0.17
Au (37 nm)	0.75 ± 0.01	11.03 ± 0.84	0.72 ± 0.05	5.90 ± 0.13
$TiCl_4$ treated Au (11 nm)	0.79 ± 0.01	17.38 ± 0.54	0.71 ± 0.01	9.73 ± 0.32

[a]The average value of each photovoltaic parameter was calculated by the three independent devices.

sphere), N is the electron density of the metal, ε_0 is the permittivity of free space, ε_∞ is the high-frequency contribution to the dielectric function, n_m is the medium RI, and m_e is the effective electron mass.[18] In our previous work,[14] we demonstrated that the LSPR wavelength is very sensitive to the RI of the surrounding medium. Experimentally, the LSPR wavelength is 533 nm while 9 nm Au NPs embedded into glass substrates (RI = 1.54), which was significantly red-shifted as compared to that (520 nm) of citrate-stabilized 10 nm Au NPs dip-coated onto ITO substrates (see Supporting Information Figure S2). Such a LSPR red-shift of 13 nm is attributed to particle−glass interfacial interactions. In the case of Au (11 nm) (Figure 4b,c), we observed that the Au NPs with (111) plane in turn have a specific bonding onto the TiO_2 (101) planes. In contrast, it is difficult to find a specific lattice in Au (19 nm) and Au (37 nm). Their Au NPs aggregate together around the NWs (Figure 2d,e). Au NPs uniformly decoded to TNWs, which significantly change the surrounding RI of Au NPs, generating a remarkable red-shift of LSPR peak in Au (11 nm). In the $TiCl_4$ treated Au (11 nm), Au NPs are covered with a TiO_2 thin layer, and the reason for the red-shift of LSPR peak to 600 nm is the same. Second, the plasmon red-shift can be

DOI: 10.1021/am507668j
ACS Appl. Mater. Interfaces 2015, 7, 1892−1898

induced by the coupling effect between Au NPs.[16,19,20] As seen in Figure 4b, most all of the gap distances between Au NPs on TNWs are around 10 nm, which is less than the particle diameter in the Au (11 nm) system. It has been proposed that when the gap distance between NPs is less than the particle diameter, a "hot spot" space can generate potentially strong localized electric fields through interparticle collective coupling, allowing a more significant red-shift.[16,19,20] Therefore, we can suggest that the LSPR red-shift of 55 nm for Au (11 nm) can also arise from a 3-D plasmon coupling effect within TNW-AuNP layer.

The photovoltaic (PV) performance of TNW-AuNP in DSSC devices is shown in Figure 5a. The resultant PV performance characterizations of open-circuit voltage (V_{oc}), short-circuit current density (J_{sc}), fill factor (FF), and efficiency (η) are listed in Table 1. Under AM 1.5 G solar illumination at 100 mW cm^{-2}, the TNW device exhibited a J_{sc} of 11.66 ± 0.32 mA cm^{-2}, a V_{oc} of 0.77 ± 0.01 V, and a FF of 0.74 ± 0.01. The η of 6.62 ± 0.10% was larger than that of the bare FTO device (η = 6.25 ± 0.15%, J_{sc} = 10.91 ± 0.76 mA cm^{-2}, V_{oc} = 0.76 ± 0.02 V, and FF = 0.76 ± 0.02). We found that the PV efficiency enhancement for TNW devices was mainly attributed to the increase in J_{sc}. Such an enhancement is due to the dual role of TNWs, AR layer and dye-absorbed layer, resulting in an improvement of light-harvesting as compared to the bare-FTO case. Therefore, we observed the dye-absorbed 600 nm nanowired TiO_2 layer exhibits absorption at 533 nm, which corresponds to the absorption of N719 (Figure 6). Moreover,

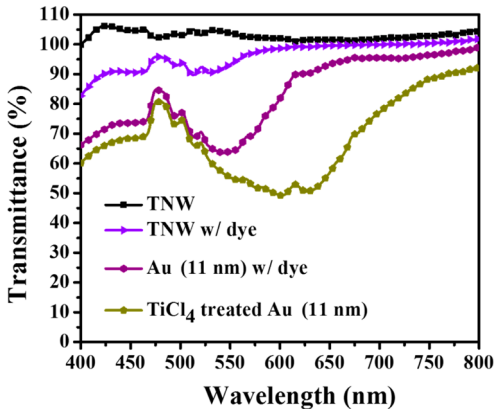

Figure 6. Transmittance spectra of dye-absorbed PFEs.

the photocurrent within the wavelength range from 380 to 800 nm increased significantly in the TNW device as illustrated in the incident photon-to-current conversion efficiency (IPCE) profile (Figure 5b). In addition, the dark current measurements show that TNWs on FTO can be a blocking layer to inhibit back electron transfer between FTO substrate and electrolyte. The onset of the dark current of the TNW devices occurred at a higher bias relative to that of the bare FTO case (bottom of Figure 5a).

As illustrated in Table 1, the best PV performance of PFE devices was achieved in the Au (11 nm). A remarkable enhancement in conversion efficiency (from 6.62% to 8.39%) by 26.7%, which is due to the significantly increased photocurrent after incorporating the Au NPs with size of 11 nm, was observed related to that based on the bare TNW device. There are three factors that can have an impact on the enhancement of photocurrents in plasmonic devices: (i) near-field effect of LSPR to enhance the light harvest, (ii) hot electron effect to generate photocurrent, and (iii) scattering effect to lengthen the optical path in the active layer.[17,21−23] To verify the contribution of the LSPR effect, the transmittance of dye-absorbed substrates (without thick TiO_2 layer) was measured. As shown in Figure 6, we can clearly find the absorption peak of N719 dye at 533 nm in a TNW electrode. The relatively broad and dramatic decline of transmittance in an Au (11 nm) substrate from 475 to 600 nm was observed, which agrees with the LSPR band position of decorated Au NPs and absorption peak of N719 dye. A dramatic decline of transmittance is because of the LSPR absorption and LSPR enhanced dye absorption. Furthermore, we further compared the curve of increase in IPCE (ΔIPCE) with the extinction spectrum of the Au (11 nm) (Figure 5c). The wavelength range, in which the IPCE values were increased, coincides with the extinction range of the Au (11 nm), suggesting that excitation of LSPR indeed improved the efficiencies. On the basis of these results, we provide evidence to conclude that the LSPR effect of Au NPs causes the enhancement of light-harvesting of N719 dye and increased photocurrent of Au (11 nm).

Also, photoelectrochemical measurement was performed to check the hot electron effect by using a three-electrode system. Figure 7 shows a photocurrent versus time curve measured

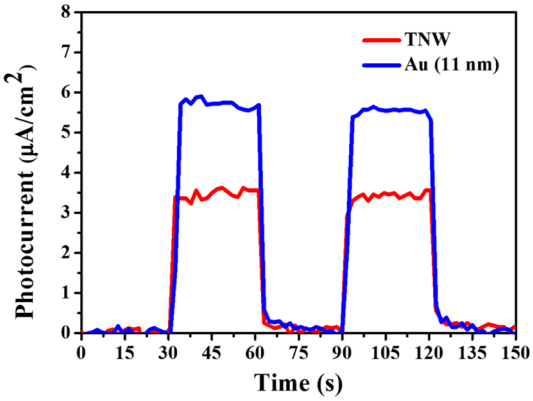

Figure 7. Chronoamperomertic $I-t$ curves collected at 0 V versus Ag/AgCl for TNW electrode and Au (11 nm) electrode under visible light illumination (using a cutoff filter with a wavelength of 400 nm).

under visible light illumination in 0.1 M NaOH electrolyte. From Figure 7, the photocurrents of TNW and Au (11 nm) electrodes are about 3 and 6 uA/cm^2, respectively. The photocurrent of TNW electrode may contribute to photo-excited electron, which absorbed the wavelength 400−420 nm. The difference in photocurrent between TNW and Au (11 nm) electrodes is attributed to hot electrons produced by the surface plasmon-induced charge separation of Au NPs, which can be injected into the conduction band of TiO_2, and lead to photocurrent generation. Although the hot electron effect can be confirmed in PFEs, the value of hot electron generated photocurrent is too tiny as compared to J_{sc}. Therefore, we judge that hot electron is not a primary affecting factor to enhance J_{sc} and efficiency.

Typically, Au NPs could also enhance the absorption in the solar cell by scattering, lengthening the optical path in the active layer. To confirm the effect of light scattering, we have performed UV−vis transmission and reflection measurement in an integrating sphere as shown in Figure 8, according to the

DOI: 10.1021/am507668j
ACS Appl. Mater. Interfaces 2015, 7, 1892−1898

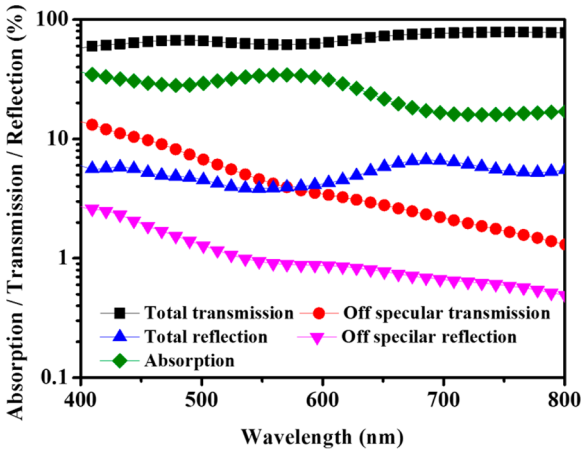

Figure 8. Absorption, transmission, and reflection spectra of Au (11 nm).

relationship A_{tot} (%) = 100 − R_{tot} − T_{tot}, where A_{tot}, R_{tot}, and T_{tot} are total absorption, total reflection, and total transmission, respectively. In the case of Au (11 nm), the T_{tot} is 61.7%, R_{tol} is 4.0%, and A_{tol} is 34.3% at the plasmonic absorbed peak 575 nm. However, the sum of the off specular transmitted (3.8%) and reflected (0.9%) light (forward and backward scattering) amounts to less than 5% as compared to 34.3% that is absorbed in the PFEs. There is 13% absorption arising from light scattering. It indicated that the scattering effect was not the primary reason for enhancement in the light absorption.

By comparison with previous reports, DSSCs based on an Au NP layer on FTO substrate exhibited an increase in the conversion efficiency from 5.84% to 6.69% while the particle size was of 25 nm.[24] Although an enhancement was demonstrated in a previous case, it is not significant. We found the reason is the weak near-field LSPR effect of 2D Au NP layer and high recombination reaction between Au/TiO_2 and electrolyte. Remarkable PV performance in Au (11 nm) device was attributed to the 3D coupling effect between Au NPs and specific binding between Au NPs and TNWs, which strengthen the near-field of LSPR resulting in enhanced light-harvesting of N719 dye. (More discussions of PV performance in the case of Au (19 nm) and Au (37 nm) were shown in Supporting Information Figure S3.) Because Au (11 nm) exhibits uniform morphology, the largest near-field coupling property, and the best cell performance as compared to others, Au (11 nm) was chosen as a candidate to further investigate.

An additional advantage for avoiding the corrosive I^-/I_3^- with Au NPs and recombination between Au and electrolyte lies in the fact that the Au NPs in Au (11 nm) were further coated with a thin TiO_2 layer using the $TiCl_4$ treatment. Comparing Figure 2c with Figure 9a, we saw the surface of TNWs and Au NPs become rough; the diameter of TNWs and Au NPs became larger after $TiCl_4$ treatment. We suggest it is because there is a thin layered TiO_2 cover on the surface of TNWs and Au NPs. From HRTEM image (Figure 9b), it is clear that the Au NPs are actually covered by a thin TiO_2 layer with a thickness about 1 nm. This thin TiO_2 layer not only acts as a protective layer but also a dye-absorbed film, which increases dye-loading and leads to more photo carrier generation. More importantly, according to the results from discrete-dipole approximation (DDA) simulation,[25] plasmonic near-fields are strongly localized close to the Au−TiO_2 interface, giving rise to a strong increase in optical absorption.[25,25,26]Thereby, the light-harvesting of dye-absorbed thin layer, which was directly covered on Au NPs, will be intensified by the LSPR effect (Figure 6), resulting in a huge enhancement in photocurrent represented in its IPCE profile (Figure 5b). Consequently, as seen in Table 1, the $TiCl_4$-treated Au (11 nm) DSSC device shows a much higher J_{sc} of 17.38 mA cm^{-2}, V_{oc} of 0.79, FF of 0.71, and yields the highest efficiency of 9.73% that has a 55.68% improvement over the performance of bare FTO-based devices (6.25%).[25]

In summary, it is well known that the narrow absorption wavelength and low absorption coefficient of N719 dye is a major problem that limits the development of DSSCs.[27] To overcome this problem, we propose a new type of PFE that can be used in different dye-absorbed DSSCs to enhance light-harvesting and cell efficiency by either AR properties of TNWs or/and plasmonic effect of Au NPs. A remarkable plasmonic red-shift from 520 to 575 nm was observed in Au (11 nm). It was attributed that Au NPs have a specific bonding interaction with TNWs, and the plasmonic electrode exhibits a strong localized electric field. We demonstrated a 55.68% improvement in the case of $TiCl_4$ treated Au (11 nm). The aforementioned superior PV performance achieved herein is mainly attributed to localized electric field improvement by plasmonic collective coupling effect within this favorable 3D TNW-AuNP hybrid nanostructure. Moreover, the fabrication

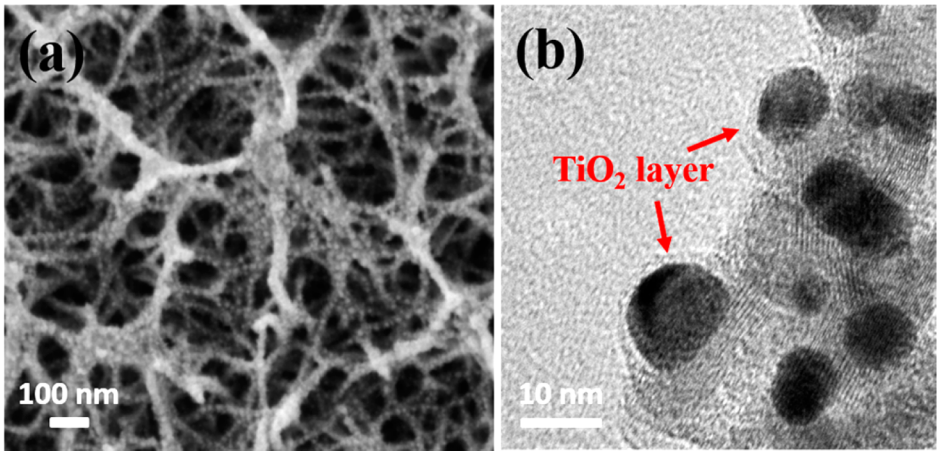

Figure 9. (a) Top-surface FESEM image and (b) HRTEM image of $TiCl_4$ treated Au (11 nm).

DOI: 10.1021/am507668j
ACS Appl. Mater. Interfaces 2015, 7, 1892−1898

technique of PFEs is inexpensive, simple, and can easily be scaled up, which is suitable for mass production. We believe this new type of PFEs will go beyond the current record of efficiency after optimization. Also, PFEs may open numerous possibilities for the use of organic solar cells, photocatalysts, and water splitting components.

EXPERIMENTAL SECTION

Preparation of TNW-AuNP Layer on FTO. The detailed synthesis method of TNWs was described in our previous work.[7] First, a 100 nm thick titanium film deposited FTO glass was treated under hydrothermal condition in a Teflon vessel with 5 M NaOH (99%, Merck) aqueous solution at 80 °C for an hour. Afterward, the substrate was washed several times with deionized water and a 0.1 M HNO_3 (65%, Merck) aqueous solution. Herein, NaOH was used as a reactive solution due to that NaOH solution has a good reactivity with Ti. Furthermore, the formation mechanism of growth of one-dimetional TiO_2 nanomaterials by using alkali hydrothermal methods based on NaOH solution had been discussed in previous publications.[28,29] After drying, the Au layer with different thickness (2.5−10 nm) was deposited onto the substrate using a sputter and then annealed at 500 °C for 30 min to fabricate the TNW-AuNP layer. The prepared TNW-AuNP FTO substrate was immersed in an aqueous solution of 50 mM $TiCl_4$ at 70 °C for 30 min followed by heat treatment at 500 °C for 30 min.

Fabrication of DSSC Devices. The photoanode was obtained by spreading TiO_2 pastes (ETERDSC Ti-2105 and ETERDSC Ti-2325) on the TNW-AuNP substrates by using the screen-printing technique. The photoanode was composed of a 7 μm-thick layer of 15−30 nm sized anatase particles and a 4 μm-thick second layer of 300 nm light-scattering TiO_2 particles. From FESEM images, we can observe that the morphology of TNW remains the same after screen-printing a TiO_2 NP layer (see Supporting Information Figure S4). After annealing at 500 °C and cooling to 80 °C, the photoanode was sensitized by immersing it in a N719 dye solution, which was prepared in a mixed acetonitrile/*tert*-butanol solution (volume ratio = 1:1) with the concentration of 3×10^{-4} M for 24 h at room temperature. The dye-absorbed photoanode was eclipsed to the Pt-sputtered counter electrodes and sealed with spacer (SX 1170-60, Solaronix SA). The electrolyte (0.05 M I_2, 0.1 M LiI, 0.6 M DMPII, and 0.5 M TBP in acetonitrile) was injected into the clamped electrodes by using a vacuum filling method. The hole was then sealed with a small square glass slide and hot-melt sealer. The detailed fabrication method can be found in our previous report.[30]

Characterizations. A Zeiss Ultraplus FESEM was used to examine the surface and cross-section morphologies of the TNWs and TNW-AuNP layer. The SigmaScan Pro 5 software was used to calculate particle size (300 particles were counted). The morphology and lattice structure of the TNW-AuNP were examined by a JEM 2010 HRTEM operated at 200 kV. A UV/vis/NIR spectrometer (Jasco v670) was used to obtain the absorption and transmittance spectra. The conversion efficiency of the solar cell was measured with a PARSTAT 2263 Advanced Electrochemical System under the illumination of solar simulator (91160A, Newport). The incident light intensities were calibrated to 1 sun with a mono-Si solar cell (AM 1.5G, 100 mW cm^{-2}). The average value of each photovoltaic parameter was calculated by three individual devices. IPCE was measured with an action spectrum measurement setup (Peccell, PEC-S20). Photoelectrochemical measurement was carried out in 0.1 M NaOH aqueous electrolyte solution at room temperature with a three-electrode cell composed of PFEs as the working electrode, platinum wire as the counter electrode, and Ag/AgCl in 1 M KCl as the reference electrode at a scan rate of 10 mV s^{-1}.

ASSOCIATED CONTENT

Supporting Information

Optical transmittance spectra and RI curve of TNW electrode; optical extinction spectra, FESEM image, and size distribution of Au NPs on glass substrate; dark-current-density−voltage curves and Nyquist plot of DSSCs; FESEM images of TNW after screen printing a thick TiO_2 film. This material is available free of charge via the Internet at http://pubs.acs.org.

AUTHOR INFORMATION

Corresponding Author

*E-mail: kjlin@dragon.nchu.edu.tw.

Notes

The authors declare no competing financial interest.

ACKNOWLEDGMENTS

We deeply appreciate the financial support of the Ministry of Science and Technology of Taiwan (NSC101-2113-M-005-014-MY3; NSC101-2628-M-007-006-MY3). We thank Prof. Yu Huang at University of California, Los Angeles, CA, for providing technical assistance in photoelectrochemical measurements. We thank Prof. Jih-Jen Wu and Wen-Pin Liao at National Cheng Kung University, Taiwan, for providing technical assistance in absorption/transmittance/scattering measurements.

REFERENCES

(1) Lee, Y.-J.; Ruby, D. S.; Peters, D. W.; McKenzie, B. B.; Hsu, J. W. P. ZnO Nanostructures as Efficient Antireflection Layers in Solar Cells. *Nano Lett.* **2008**, *8*, 1501−1505.

(2) Striemer, C. C.; Fauchet, P. M. Dynamic Etching of Silicon for Broadband Antireflection Applications. *Appl. Phys. Lett.* **2002**, *81*, 2980−2982.

(3) Mavrokefalos, A.; Han, S. E.; Yerci, S.; Branham, M. S.; Chen, G. Efficient Light Trapping in Inverted Nanopyramid Thin Crystalline Silicon Membranes for Solar Cell Applications. *Nano Lett.* **2012**, *12*, 2792−2796.

(4) Zhu, J.; Yu, Z.; Burkhard, G. F.; Hsu, C.-M.; Connor, S. T.; Xu, Y.; Wang, Q.; McGehee, M.; Fan, S.; Cui, Y. Optical Absorption Enhancement in Amorphous Silicon Nanowire and Nanocone Arrays. *Nano Lett.* **2008**, *9*, 279−282.

(5) Richards, B. S.; Rowlands, S. F.; Honsberg, C. B.; Cotter, J. E. TiO_2 DLAR Coatings for Planar Silicon Solar Cells. *Prog. Photovoltaics* **2003**, *11*, 27−32.

(6) Aurang, P.; Demircioglu, O.; Es, F.; Turan, R.; Unalan, H. E. ZnO Nanorods as Antireflective Coatings for Industrial-Scale Single-Crystalline Silicon Solar Cells. *J. Am. Ceram. Soc.* **2013**, *96*, 1253−1257.

(7) Chen, J.-Z.; Ko, W.-Y.; Yen, Y.-C.; Chen, P.-H.; Lin, K.-J. Hydrothermally Processed TiO_2 Nanowire Electrodes with Antireflective and Electrochromic Properties. *ACS Nano* **2012**, *6*, 6633−6639.

(8) Li, Y.; Wang, H.; Feng, Q.; Zhou, G.; Wang, Z.-S. Gold Nanoparticles Inlaid TiO_2 Photoanodes: a Superior Candidate for High-Efficiency Dye-Sensitized Solar Cells. *Energy Environ. Sci.* **2013**, *6*, 2156−2165.

(9) Yu, K.; Tian, Y.; Tatsuma, T. Size Effects of Gold Nanaoparticles on Plasmon-Induced Photocurrents of Gold-TiO_2 Nanocomposites. *Phys. Chem. Chem. Phys.* **2006**, *8*, 5417−5420.

(10) Muduli, S.; Game, O.; Dhas, V.; Vijayamohanan, K.; Bogle, K. A.; Valanoor, N.; Ogale, S. B. TiO_2−Au Plasmonic Nanocomposite for Enhanced Dye-Sensitized Solar Cell (DSSC) Performance. *Sol. Energy* **2012**, *86*, 1428−1434.

(11) Jang, Y. H.; Jang, Y. J.; Kochuveedu, S. T.; Byun, M.; Lin, Z.; Kim, D. H. Plasmonic Dye-Sensitized Solar Cells Incorporated with Au-TiO_2 Nanostructures with Tailored Configurations. *Nanoscale* **2014**, *6*, 1823−1832.

(12) Zarick, H. F.; Hurd, O.; Webb, J. A.; Hungerford, C.; Erwin, W. R.; Bardhan, R. Enhanced Efficiency in Dye-Sensitized Solar Cells with

DOI: 10.1021/am507668j
ACS Appl. Mater. Interfaces 2015, 7, 1892−1898

Shape-Controlled Plasmonic Nanostructures. *ACS Photonics* **2014**, *1*, 806−811.
(13) Wang, H.; You, T.; Shi, W.; Li, J.; Guo, L. Au/TiO_2/Au as a Plasmonic Coupling Photocatalyst. *J. Phys. Chem. C* **2012**, *116*, 6490−6494.
(14) Hsu, C.-Y.; Huang, J.-W.; Gwo, S.; Lin, K.-J. The Facile Fabrication of Tunable Plasmonic Gold Nanostructure Arrays Using Microwave Plasma. *Nanotechnology* **2010**, *21*, 035302−035306.
(15) Kelly, K. L.; Coronado, E.; Zhao, L. L.; Schatz, G. C. The Optical Properties of Metal Nanoparticles: The Influence of Size, Shape, and Dielectric Environment. *J. Phys. Chem. B* **2002**, *107*, 668−677.
(16) Kawawaki, T.; Takahashi, Y.; Tatsuma, T. Enhancement of Dye-Sensitized Photocurrents by Gold Nanoparticles: Effects of Plasmon Coupling. *J. Phys. Chem. C* **2013**, *117*, 5901−5907.
(17) Atwater, H. A.; Polman, A. Plasmonics for Improved Photovoltaic Devices. *Nat. Mater.* **2010**, *9*, 205−213.
(18) Jain, P. K.; El-Sayed, M. A. Noble Metal Nanoparticle Pairs: Effect of Medium for Enhanced Nanosensing. *Nano Lett.* **2008**, *8*, 4347−4352.
(19) Hartland, G. V. Optical Studies of Dynamics in Noble Metal Nanostructures. *Chem. Rev.* **2011**, *111*, 3858−3887.
(20) Ghosh, S. K.; Pal, T. Interparticle Coupling Effect on the Surface Plasmon Resonance of Gold Nanoparticles: From Theory to Applications. *Chem. Rev.* **2007**, *107*, 4797−4862.
(21) Wen, C.; Ishikawa, K.; Kishima, M.; Yamada, K. Effects of Silver Particles on the Photovoltaic Properties of Dye-Sensitized TiO_2 Thin Films. *Sol. Energy Mater. Sol. Cells* **2000**, *61*, 339−351.
(22) Tian, Y.; Tatsuma, T. Mechanisms and Applications of Plasmon-Induced Charge Separation at TiO_2 Films Loaded with Gold Nanoparticles. *J. Am. Chem. Soc.* **2005**, *127*, 7632−7637.
(23) Wu, J.-L.; Chen, F.-C.; Hsiao, Y.-S.; Chien, F.-C.; Chen, P.; Kuo, C.-H.; Huang, M. H.; Hsu, C.-S. Surface Plasmonic Effects of Metallic Nanoparticles on the Performance of Polymer Bulk Heterojunction Solar Cells. *ACS Nano* **2011**, *5*, 959−967.
(24) Zhang, D.; Wang, M.; Brolo, A. G.; Shen, J.; Li, X.; Huang, S. Enhanced Performance of Dye-Sensitized Solar Cells Using Gold Nanoparticles Modified Fluorine Tin Oxide Electrodes. *J. Phys. D: Appl. Phys.* **2013**, *46*, 024005.
(25) Seh, Z. W.; Liu, S.; Low, M.; Zhang, S.-Y.; Liu, Z.; Mlayah, A.; Han, M.-Y. Janus Au-TiO_2 Photocatalysts with Strong Localization of Plasmonic Near-Fields for Efficient Visible-Light Hydrogen Generation. *Adv. Mater.* **2012**, *24*, 2310−2314.
(26) Cheng, Y. Y.; Fuckel, B.; MacQueen, R. W.; Khoury, T.; Clady, R. G. C. R.; Schulze, T. F.; Ekins-Daukes, N. J.; Crossley, M. J.; Stannowski, B.; Lips, K.; Schmidt, T. W. Improving the Light-Harvesting of Amorphous Silicon Solar Cells with Photochemical Upconversion. *Energy Environ. Sci.* **2012**, *5*, 6953−6959.
(27) Hardin, B. E.; Hoke, E. T.; Armstrong, P. B.; Yum, J.-H.; Comte, P.; Torres, T.; Frechet, J. M. J.; Nazeeruddin, M. K.; Gratzel, M.; McGehee, M. D. Increased Light Harvesting in Dye-Sensitized Solar Cells with Energy Relay Dyes. *Nat. Photonics* **2009**, *3*, 406−411.
(28) Dong, W.; Zhang, T.; Epstein, J.; Cooney, L.; Wang, H.; Li, Y.; Jiang, Y.-B.; Cogbill, A.; Varadan, V.; Tian, Z. R. Multifunctional Nanowire Bioscaffolds on Titanium. *Chem. Mater.* **2007**, *19*, 4454−4459.
(29) Yada, M.; Inoue, Y.; Uota, M.; Torikai, T.; Watari, T.; Noda, I.; Hotokebuchi, T. Plate, Wire, Mesh, Microsphere, and Microtube Composed of Sodium Titanate Nanotubes on a Titanium Metal Template. *Langmuir* **2007**, *23*, 2815−2823.
(30) Chen, J.-Z.; Yen, Y.-C.; Ko, W.-Y.; Cheng, C.-Y.; Lin, K.-J. The Role of the Fabrication of Anatase-TiO_2 Chain-Networked Photoanodes. *Adv. Mater.* **2011**, *23*, 3970−3973.

DOI: 10.1021/am507668j
ACS Appl. Mater. Interfaces 2015, 7, 1892−1898